

RETHINKING THE VULNERABILITY OF CONCEPT ERASURE AND A NEW METHOD

Anonymous authors

Paper under double-blind review

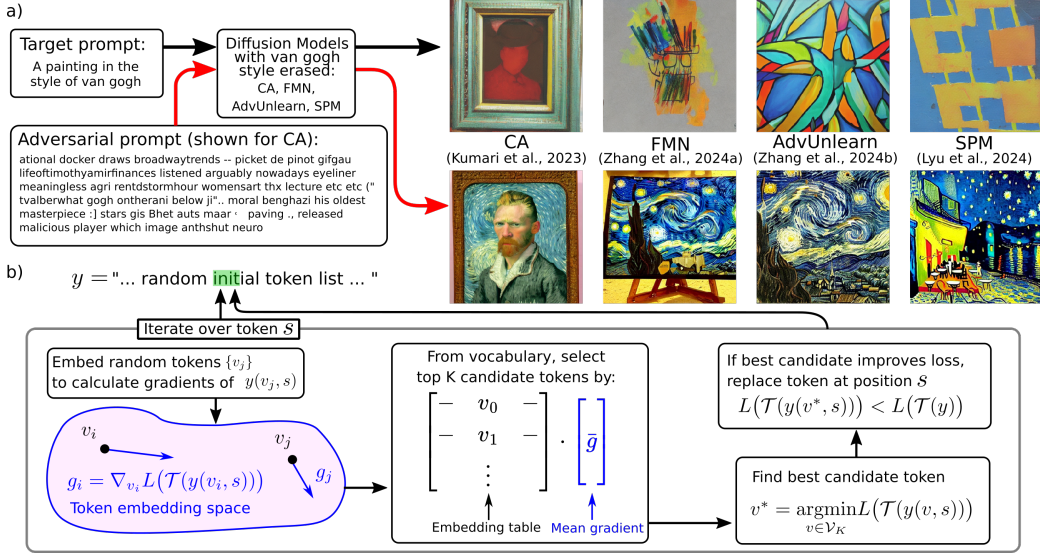


Figure 1: **a)** Examples images from models unlearned on van Gogh painting style. **b)** The update schematic of RECORD, which uses a linear gradient approximation to obtain a small set of candidate tokens, and then updates the prompt with respect to the exact evaluation of the loss function.

ABSTRACT

The proliferation of text-to-image diffusion models has raised significant privacy and security concerns, particularly regarding the generation of copyrighted or harmful images. In response, concept erasure (defense) methods have been developed to "unlearn" specific concepts through post-hoc finetuning. However, recent concept restoration (attack) methods have demonstrated that these supposedly erased concepts can be recovered using adversarially crafted prompts, revealing a critical vulnerability in current defense mechanisms. In this work, we first investigate the fundamental sources of adversarial vulnerability and reveal that vulnerabilities are pervasive in the prompt embedding space of concept-erased models, a characteristic inherited from the original pre-unlearned model. Furthermore, we introduce **RECORD**, a novel coordinate-descent-based restoration algorithm that consistently outperforms existing restoration methods by up to 17.8 times. We conduct extensive experiments to assess its compute-performance tradeoff and propose acceleration strategies. The code for RECORD is available at [available upon publication].

Note: this paper may contain offensive or upsetting images

1 INTRODUCTION

Text-to-Image Diffusion models have recently garnered significant attention for their ability to generate high-quality images from natural language inputs (Song et al., 2020; Rombach et al., 2022). However, because these models are trained on vast and diverse datasets that may contain harmful

054 or undesirable content, their proliferation raises substantial ethical and safety concerns, particularly
055 over the generation of copyrighted and harmful content (Chin et al., 2023; Somepalli et al., 2022).
056 Pre-filtering undesired images from the training dataset is often considered impractical due to the
057 sheer size of these datasets, as well as the cost of re-training models from scratch. Consequently,
058 much research has pursued post-hoc approaches aiming to remove the undesired content from trained
059 models via low-cost finetuning, while preserving the generation quality of other non-erased concepts
060 (Gandikota et al., 2023a; Wu et al., 2024; Wu & Harandi, 2024; Zhang et al., 2024a; Kumari et al.,
061 2023; Lyu et al., 2024; Fan et al., 2023; Gandikota et al., 2023b; Zhang et al., 2024b; Gong et al.,
062 2024; Kim et al., 2024; Zhang et al., 2025; Gao et al., 2024; Srivatsan et al., 2025). This is commonly
063 referred to as *concept erasure*, a subfield of *machine unlearning* (Kim & Qi, 2025).

064 However, it is well-known that neural networks are susceptible to adversarial attacks: small pertur-
065 bations to an input can induce a well-trained model to produce any pre-determined outputs without
066 altering the model itself (Kurakin et al., 2016; Dong et al., 2018; Yang et al., 2024; Beerens &
067 Higham, 2024). This vulnerability raises similar concerns in the context of concept erasure. Indeed,
068 recent studies have largely demonstrated the feasibility of eliciting unlearned models to re-generate
069 the erased concepts via white-box optimization-based attacks (Chin et al., 2023; Zhang et al., 2023).
070 We refer to this class of attack methods as *concept restoration*.

071 While the success of concept restoration methods demonstrates the vulnerability of concept-erased
072 models, the underlying cause of this persistent susceptibility to adversarial attacks is not yet fully
073 understood (Lu et al., 2025). To this end, our investigations reveal crucial insights into the fundamental
074 vulnerability of unlearned models. Notably, prompt embeddings initialized in different regions of
075 the embedding space, our findings suggest there often exist nearby embeddings that can restore the
076 erased concepts. This suggests adversarial embeddings are pervasive in the prompt embedding space
077 and can be exploited by the existing restoration algorithms. Furthermore, for certain types of erasure
078 methods, embeddings initialized near the exact descriptions of the erased concept tend to diverge
079 from those embeddings during optimization. This suggests that most existing unlearning methods
080 only suppress the generation of the erased concept under prompts embedded near the specific prompt
081 embeddings corresponding to the erased concept.

082 Stemming from these findings, we notice existing concept restoration methods rely on projecting
083 the discrete text prompts into a continuous and differentiable space to enable gradient-based opti-
084 mization (Chin et al., 2023; Zhang et al., 2023). However, recent studies have demonstrated that
085 projection-based adversarial attacks generally underperform in comparison to coordinate-descend-
086 based approaches (Carlini et al., 2023; Zou et al., 2023; Jones et al., 2023) in language model
087 adversarial attacks. This motivates our investigation of similar approaches in the field of concept
088 restoration. Therefore, we further propose **RECORD** (**R**estoring **E**rased **C**oncepts via **C**oordinate
089 **D**escent), a white-box coordinate-descent algorithm employing a two-stage optimization scheme to
090 negate the need for projection (Figure 1). Our extensive experiments demonstrated that RECORD con-
091 sistently achieve superior performance by up to 17.8-fold over the existing state-of-the-art restoration
092 methods. Examples of the restored images are presented in Table 1.

093 The contributions of this paper are as follows:

094 • We explore why the majority of the current concept erasure methods are largely susceptible to
095 concept restoration attacks.

096 • We extend the existing concept restoration attack methods by introducing RECORD, a coordinate
097 descent approach motivated by similar successes on language model adversarial attacks.

098 • We conduct extensive ablation studies on RECORD, carefully assessing the effect of each hyperpa-
099 rameter and revealing its highly flexible compute-performance tradeoffs.

100 2 BACKGROUND

101 2.1 TEXT-TO-IMAGE DIFFUSION MODELS

102 Diffusion Models are a class of generative model that generate images from text by learning to
103 reverse the forward diffusion process. Starting with Gaussian noise $x_T \sim \mathcal{N}(0, 1)$, a trained denoiser,
104 commonly a U-Net (Ronneberger et al., 2015) or Vision Transformer (Dosovitskiy et al., 2020),
105 iteratively denoises x_T over the interval $t \in [0, T]$ until a clear image x_0 is reached. By conditioning

Restoration Method	Erasure Method					
	ESD 2023a	FMN 2024a	AC 2023	SPM 2024	UCE 2023b	AdvUnlearn 2024b
P4D 2023						
UD 2023						
RECORD						

Table 1: Example images of erased concepts (van Gogh painting style) using token-level attacks. Each image column of the same concept is generated using the same latent initialization.

on prompt embeddings $c = \mathcal{T}(y)$, where y is some natural language prompt, text-to-image generation is achieved. \mathcal{T} is a pre-trained text encoder, commonly CLIP (Radford et al., 2021) or BLIP (Li et al., 2022). Latent diffusion models, such as Stable Diffusion (Rombach et al., 2022), perform the denoising in latent space $z_t = \mathcal{E}(x_t)$ and the denoiser ϵ_θ is trained with the following objective

$$\operatorname{argmin}_\theta \mathbb{E}_{z \sim \mathcal{E}(x), t, \epsilon \sim \mathcal{N}(0, 1), c} \|\epsilon - \epsilon_\theta(z_t, t, c)\|_2^2.$$

where z_t is obtained from the forward diffusion process to the clean latent z_0 with Gaussian noise ϵ .

2.2 PROMPT TUNING

Manipulating prompts to elicit specific behaviors from language models, also known as prompt tuning, is an important topic in Natural Language Processing research. (Ebrahimi et al., 2018) introduced HotFlip, generating adversarial examples through minimal character-level flips guided by gradients. Extending this, (Wallace et al., 2021) developed Universal Adversarial Triggers—input-agnostic token sequences optimized by using first order Taylor-expansion around the current token to select candidate tokens for exact evaluation. (Shin et al., 2020) presented AutoPrompt, designed to automatically generate prompts for various use cases. Addressing the lack of fluency in these prompts, (Shi et al., 2022) introduced FluentPrompt, incorporating fluency constraints and using Langevin Dynamics combined with Projected Stochastic Gradient Descent, where projection is done onto the set of token embeddings. (Wen et al., 2023) developed PEZ, an algorithm inspired by FluentPrompt, allowing for prompt creation in both text-to-text and text-to-image applications. In text-to-image models, (Gal et al., 2022) applied Textual Inversion, learning "pseudo-words" in the embedding space to capture specific visual concepts. Further advancements include GBDA (Guo et al., 2021), enabling gradient-based optimization over token distributions using the Gumbel-Softmax reparametrization (Jang et al., 2017) to stay on the probability simplex, GCG (Zou et al., 2023) and ARCA (Jones et al., 2023), optimizing discrete prompts via an improvement to AutoPrompt. ARCA will inspire our method.

2.3 CONCEPT RESTORATION

Recent methods for restoring erased concepts from unlearned models often leverage advanced optimization techniques similar to prompt tuning. Concept Inversion (CI) (Pham et al., 2023) introduces a new token with learnable embedding to represent the erased concept, which is learned to minimize the reconstruction loss during denoising. This is a direct application of Textual Inversion (Gal et al., 2022) from prompt tuning to the concept restoration paradigm. Prompting Unlearned Diffusion Models (PUND) (Han et al., 2024) enhances this approach by iteratively erasing

162 and searching for the concept while also updating model parameters, improving transferability across
163 models.

164 Other methods focus on discrete token optimization. UnlearnDiffAtk (UD) (Zhang et al., 2023)
165 performs optimization over token distributions, similar to GBDA (Guo et al., 2021), but utilizes
166 projection onto the probability simplex instead of the Gumbel-Softmax reparameterization. Prompt-
167 ing4Debugging (P4D) (Chin et al., 2023) optimizes prompts in the embedding space and projects
168 onto discrete embeddings, akin to the approach used in PEZ (Wen et al., 2023). Additionally, Ring-
169 A-Bell (Tsai et al., 2023) constructs an empirical representation of the erased concept by averaging
170 embedding differences from prompts with and without the concept, then employs a genetic algorithm
171 to optimize the prompt.

173 3 METHODS

174 3.1 MOTIVATION

175 Verifying whether a model has truly unlearned a concept is challenging. To assess the effectiveness
176 of the unlearning process, we consider an unlearned denoiser $\epsilon_{\theta'}$ to be robust if it consistently fails to
177 generate the erased content and produce images significantly different from those generated by the
178 original model ϵ_{θ} when subjected to any adversarial prompt and any latent initialization. Therefore,
179 this work focuses on measuring the degree to which the unlearned model has diverged from the
180 original model concerning the erased content. To achieve this, we propose a loss function similar to
181 (Chin et al., 2023)

$$184 L(c) = \mathbb{E}_{t,z} \left[\left\| \epsilon_{\theta'}(z_t, t, c) - \epsilon_{\theta}(z_t, t, c_{\text{target}}) \right\|_2^2 \right], \quad (1)$$

185 where $c = \mathcal{T}(y)$, $c_{\text{target}} = \mathcal{T}(y_{\text{target}})$, z_t is obtained through the forward diffusion process with z_0
186 sampled from the target data distribution p_{target} . y_{target} is the target prompt. The subsequent concept
187 restoration attacks can be performed by minimizing this loss and finding the adversarial text prompt

$$189 y^* = \underset{y}{\operatorname{argmin}} L(\mathcal{T}(y)).$$

190 This formulation is similarly applicable to erasure methods which unlearns the text encoder \mathcal{T} . This
191 paper considers two types of restoration attacks to assess the vulnerability of unlearned models:

- 192 • **Embedding-level attacks:** In this setting, concept restoration is achieved by directly perturbing
193 the prompt embedding c to minimize the loss function defined in Equation [1]. With the prompt
194 embedding space being continuous and differentiable, finding adversarial prompts poses an easier
195 task. However, precise inversions from embeddings back to prompts are not guaranteed to exist,
196 making embedding-level attacks less practicable and realistic in most circumstances.
- 197 • **Token-level attacks:** Directly perturbing prompt tokens to restore concepts is significantly more
198 challenging due to their discrete and non-differentiable nature. To overcome this limitation, we
199 introduce **RECORD** for carrying out robust concept restoration attacks.

201 3.2 EMBEDDING-LEVEL ATTACKS: A PEEK INTO THE ORIGIN OF MODEL VULNERABILITY

202 Embedding-level attacks for restoring the erased concept can be easily carried out in a naive approach
203 of directly optimizing on the prompt embedding c with a fixed learning rate. Since computing the
204 exact expectation over all latents and timesteps is intractable, we approximate the $L(y)$ from Equation
205 [1] as:

$$207 \hat{L}(c, \mathcal{Z}) = \sum_{(z_t, t) \in \mathcal{Z}} \left\| \epsilon_{\theta'}(z_t, t, c) - \epsilon_{\theta}(z_t, t, \mathcal{T}(y_{\text{target}})) \right\|_2^2, \quad (2)$$

208 where \mathcal{Z} is a sampled batch of noised images and their corresponding timesteps. For embedding-level
209 attacks, we use a batch size of 16 images and NAdam for optimizing onprompt embedding c with a
210 fixed learning rate of 0.1. The full embedding-level attack results can be found in Appendix B.

211 To explore vulnerability, we visualize the 2D isomap (Wang, 2012) projections of prompt embedding
212 optimization trajectories (Figure 2a), providing a visual intuition for their flow within the embedding
213 space. We use an exact description of the erased concept as the reference target, e.g. "a painting in
214 the style of van Gogh" for models unlearned on van Gogh art style, and investigate four different

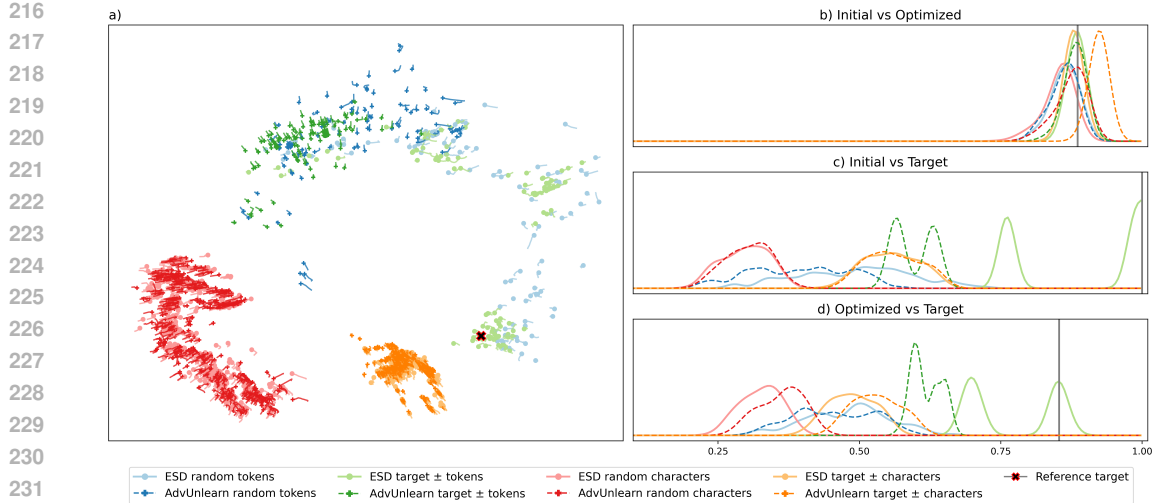


Figure 2: Behavior of the text embeddings during embedding-level attacks on models unlearned with ESD and AdvUnlearn. **a)** Isomap projection of the optimization trajectories in the prompt embedding space $\mathbb{R}^{T \times 77 \times 768}$ down to $\mathbb{R}^{T \times 2}$. 2000 trajectories shown, each $T = 10$ steps long. Dots / crosses denote the starting point. The erased concept can be generated at the end of each trajectory. **b), c), d)** present the cosine similarity histogram, computed in $\mathbb{R}^{77 \times 768}$, between the initial, optimized, and reference target embeddings.

initialization schemes: Prompt embeddings initialized "close" to the reference target of the erased concept by padding and replacing random tokens (\pm tokens) or characters (\pm characters) of random lengths; Prompt embeddings initialized "far" from the reference target by uniformly sampling random tokens or characters. Remarkably, embeddings initialized in all four regions of the embedding space can successfully restore the erased concept with short optimization trajectories (Figure 2a and 2b). In particular, embeddings initialized in the far region can generate the erased concept without approaching the region close to the reference target embedding. This suggests that, there often locally exists an adversarial prompt embedding close to the initialization. In other words, unlearned models are generally vulnerable to small perturbations to the text embedding, and effective adversarial embeddings are widespread in the prompt embedding space. This echoes the well-established understanding that neural networks are adversarially vulnerable to small perturbation to its inputs (Fawzi et al., 2018; Simon-Gabriel et al., 2018; Wu et al., 2020; Beerens & Higham, 2024).

For denoiser-based erasure methods like ESD (Gandikota et al., 2023a), embeddings initialized "close" to the target embedding tend to diverge from the reference target embedding during optimization (Figure 2c and 2d). This suggests that denoiser-based erasure methods only suppress generation of a concept in a localized region around the reference target embedding. By contrast, for methods that unlearn the text encoders, such as AdvUnlearn (Zhang et al., 2024b), embeddings tend to converge slightly towards yet still remain far away from the reference target. This dynamic indicates a different failure mode: modifying the text encoder alters the token-embedding mapping but does not necessarily erase the model's inherent ability to generate the concept from embeddings located in that specific region.

Collectively, these results demonstrate that embedding-level vulnerabilities are ubiquitous and remain largely unaddressed except in some specific regions of the embedding space. The pervasive nature of these embeddings make the concept-erased models susceptible to exploitation by token-level restoration algorithms. Conversely, for erasure methods that are more robust to embedding-level attacks, such as SH (Wu & Harandi, 2024) (see Appendix B), token-level attacks are also likely to underperform. Building on this, we further elaborate in Appendix A that the pervasiveness of these vulnerabilities is not an artifact of the concept erasure process, but inherited from the original pre-unlearned model: *it is possible to find local embeddings for generating a target concept even when initializing from a semantically distant starting point.*

Algorithm 1 Pseudocode of RECORD.

```

271 #  $\theta'$ : original model;  $\theta$ : unlearned model
272 #  $y_{\text{target}}$ : target prompt
273 #  $J$ : gradient samples;  $K$ : candidates
274 #  $S$ : sequence length;  $N$ : passes
275 #  $R$ : reference set;  $E$ : embedding table
276
277 Random token sequence  $y$  of length  $S$ : # initialization
278 for n=1 to N: # load N passes
279     # Shuffle
280     Random permutation  $\pi$  of positions  $\{1, \dots, S\}$ 
281
282     for  $s$  in  $\pi$ :
283         # sample data
284         Sample batch  $\mathcal{Z}$  of noise images and timesteps
285         # candidate selection
286             Sample  $J$  random tokens  $\{v_j\}$ 
287             Compute gradients  $\bar{g} = \frac{1}{J} \sum_{j=1}^J \nabla v_j \hat{L}(\mathcal{T}(y(v_j, s)), \mathcal{Z}(n, s))$ 
288             Score all tokens: scores  $\leftarrow E\bar{g}$ 
289             Select top  $K$  tokens  $\mathcal{V}$  based on scores
290
291         # candidate evaluation
292          $\hat{v}^* = \arg \min_{v \in \mathcal{V}} \hat{L}(y(v, s), \mathcal{Z})$  # best candidate
293         # coordinate descent
294         if  $\hat{L}(\mathcal{T}(y(\hat{v}^*, s)), \mathcal{R}) < \hat{L}(\mathcal{T}(y), \mathcal{R})$ :
295             Update  $y \leftarrow y(\hat{v}^*, s)$ 
296
297 Return: optimized prompt  $y$  for restoring erased concepts

```

3.3 TOKEN-LEVEL ATTACKS: NEW METHOD

Existing concept restoration methods use gradient-based optimization, which necessitates the projection of the non-differentiable discrete text prompts to a continuous and differentiable space (Chin et al., 2023; Zhang et al., 2023). However, recent studies have observed superior performance of coordinate-descend-based methods over their projection counterparts when optimizing on discrete texts (Carlini et al., 2023; Zou et al., 2023; Jones et al., 2023). This motivates us to introduce RECORD, a coordinate descent approach that iteratively optimizes the prompt by refining one token at a time while fixing all other tokens. A naive implementation of this strategy requires evaluating the loss function for every token in the vocabulary at each position, which quickly becomes intractable for large vocabularies. To make this optimization feasible, RECORD uses a two-stage approach of leveraging a linear approximation of the loss gradient to identify a small subset of candidate tokens, then perform exact evaluations to determine the optimal token for substitution.

More precisely, the algorithm first initializes a random token sequence $y = [y_1, \dots, y_S]$ of length S , and iteratively performs N passes over y . In each pass, a random permutation of the token positions is generated to mitigate positional bias during updates. For each position s in the permuted sequence, the algorithm samples a batch of clean latents $z_0^{[n]}$ and corresponding timesteps $t^{[n,s]}$. Candidate tokens v for position s are then selected by sampling J random tokens, and computing the gradient g of the loss \hat{L} from Equation [2] with respect to the candidate token embeddings:

$$g_j = \nabla v_j \hat{L}(\mathcal{T}(y(v_j, s)), \mathcal{Z}(n, s)).$$

The average gradient $\bar{g} = \frac{1}{J} \sum_{j=1}^J g_j$ serves as a linear approximation to \hat{L} with respect to the entire prompt embedding space. By multiplying the embedding table E with \bar{g} , we efficiently score all possible tokens and select the top K candidates for exact evaluation. This effectively alleviates the intractability introduced by the large vocabulary in the naive approach. During the evaluation and subsequent update of y_s , we employ a greedy strategy: a candidate token \hat{v}^* is only accepted if it improves the loss, i.e. when $\hat{L}(\mathcal{T}(y(\hat{v}^*, s)), \mathcal{R}) < \hat{L}(\mathcal{T}(y), \mathcal{R})$, where \mathcal{R} is the reference set. This update process iterates through all positions in the permutation and repeats for N passes, progressively enhancing the token sequence over time. Since each accepted token replacement strictly decreases the loss and the number of possible token sequences is finite, the algorithm is guaranteed to converge to a coordinate-wise local minimum. A pseudocode can be found in Algorithm 1.

Although the RECORD algorithm as described above is tailored for attacking denoiser-based erasure methods, it can be easily adapted to text-encoder-based erasure methods by replacing \mathcal{T} with \mathcal{T}' in \hat{L} when encoding y , where \mathcal{T}' is the unlearned text encoder.

Erased concept	van Gogh	Church	Garbage Truck	Parachute	Nudity
Accuracy	99.4	98.8	93.4	84.0	87.6

324
325 Table 2: The classification accuracy of Stable Diffusion 2.1 as a zero-shot image classifier
326
327

331 **4 EXPERIMENTS**
332

334 We designed our experiments to address the following questions:
335

- 336 1. Does the proposed RECORD algorithm outperform current SOTA concept restoration methods?
337
- 338 2. Are certain concept erasure methods more robust?
339
- 340 3. How important are the different RECORD hyperparameters?
341

342 We extensively compare RECORD against the two current state-of-the-art concept restoration methods
343 in the literature, P4D (Chin et al., 2023) and UD (Zhang et al., 2023), on text-to-image diffusion
344 models unlearned with both denoiser-based (ESD (Gandikota et al., 2023a), ED (Wu et al., 2024),
345 SH (Wu & Harandi, 2024), FMN (Zhang et al., 2024a), CA (Kumari et al., 2023), SPM (Lyu et al.,
346 2024), SalUn (Fan et al., 2023), UCE (Gandikota et al., 2023b), and RECE (Gong et al., 2024)) and
347 text-encoder-based (AdvUnlearn (Zhang et al., 2024b)) concept erasure methods. Although there are
348 other black-box methods that suppress generation of harmful content without post-hoc training the
349 denoiser or the text encoder (Yoon et al., 2024; Schramowski et al., 2023; Li et al., 2024; Jain et al.,
350 2024), such methods target a fundamentally different adversary, e.g. one with only API access, and
351 cannot exploit internal gradients or weights of the unlearned model. Including them here would not
352 yield an apple-to-apple evaluation of concept erasure under full model access. We use open-sourced
353 unlearned model weights from (Zhang et al., 2024b; Gong et al., 2024), which uses Stable Diffusion
354 1.4 (SD1.4) (Rombach et al., 2022) as the base model. The erased concepts include art style (van
355 Gogh), objects (church, garbage truck, parachute) and nudity.
356

357 **4.1 EVALUATION METRIC**
358

359 Most text-to-image diffusion models can generate a far broader range of objects and styles than any
360 single image classifier is capable of classifying. Prior work therefore evaluates concept erasure and
361 restoration methods by ensembling multiple classifiers, each with its own architecture, training data,
362 and preprocessing method, introducing potential inconsistencies. To address this issue, as well as to
363 improve reproducibility and ease replication, we adopt a single, unified zero-shot diffusion classifier
364 (Stable Diffusion v2.1) (Li et al., 2023; Clark & Jaini, 2023). The classification results are obtained
365 by computing

$$366 \quad y^* = \operatorname{argmin}_{y_i \in Y} \mathbb{E}_t \|\epsilon - \epsilon_\theta(z_t, t, \mathcal{T}(y_i))\|_2^2,$$

367 where the timestep t is uniformly sampled from $U(0, T)$, $Y = \{y_1, y_2, \dots, y_n\}$ is a set of n
368 classification classes. The expectation is computed over 10 samples, which in our experience is
369 sufficient to provide accurate classification results. For art style and object attacks, we build sets of 50
370 classes using prompt templates ‘a painting in the style of {artist_name}’ and ‘a photorealistic image
371 of {object}’, where the artist names are randomly chosen from a list of famous painters, e.g. Leonardo
372 Da Vinci, and object names are from the classification classes of YOLOv3 (Redmon & Farhadi,
373 2018). For nudity attacks, a set of 4 classes are built with the same template as the object attacks. For
374 all attacks, we also additionally add one empty class, ‘’, which helps the classifier capture images
375 that fall significantly outside the distributions of the specified classes. All results presented in this
376 section are computed on 500 images generated by the corresponding erased models and restoration
377 attacks. We report the Attack Success Rate (ASR) in percentage, calculated by dividing the number
378 of images classified as the target (erased) class by the total number of generated images. We attach
379 the classification accuracy of the zero-shot diffusion classifier on images generated by the baseline
380 model in Table 2, which serves as references for the ASRs of the corresponding concepts.
381

Erased Concept	Restoration Method	Erasure Method						
		ESD 2023a	FMN 2024a	AC 2023	SPM 2024	UCE 2023b	AdvUnlearn 2024b	RECE 2024
van Gogh	P4D 2023	6.6	27.2	49.8	54.8	67.2	2.8	50.8
	UD 2023	5.4	25.4	17.0	34.6	42.8	2.8	10.0
	RECORD	64.0	76.8	94.0	95.6	97.6	33.0	89.0
Erased Concept	Restoration Method	Erasure Method						
		ED 2024	ESD 2023a	SalUn 2023	SH 2024	SPM 2024	AdvUnlearn 2024b	RECE 2024
Church	P4D 2023	16.0	24.6	28.8	3.4	51.6	7.0	8.2
	UD 2023	2.6	4.8	5.4	4.4	22.8	1.4	6.8
	RECORD	61.2	75.2	71.4	8.6	92.2	57.0	46.4
Garbage Truck	P4D 2023	9.4	18.8	21.0	0.4	35.8	34.2	5.6
	UD 2023	16.0	3.8	17.0	4.4	29.2	0.2	1.2
	RECORD	40.8	38.8	58.0	1.0	66.4	50.0	17.0
Parachute	P4D 2023	5.6	11.6	20.6	0.6	15.6	2.0	4.2
	UD 2023	3.0	2.4	2.4	1.0	6.8	1.2	3.2
	RECORD	15.4	44.6	48.8	2.0	60.4	35.6	10.0
Nudity	P4D 2023	2.0	37.6	9.8	9.6	28.8	17.0	15.2
	UD 2023	4.0	19.2	4.2	2.0	2.5	14.2	19.4
	RECORD	2.4	70.6	9.0	21.2	69.0	39.2	38.8

Table 3: Attack success rate (%) for models erased on different concepts (van Gogh style, Church, Garbage Truck, Parachute, Nudity), compared with different restoration methods P4D (Chin et al., 2023), UD (Zhang et al., 2023), and RECORD. The best and second-best values are marked in red and gray, respectively.

4.2 RESULTS

In this experiment, each restoration method (P4D (Chin et al., 2023), UD (Zhang et al., 2023), RECORD) aims to find 64-token-long seed-agnostic adversarial prompts starting from a randomly initialized prompt sequence, except UD. Since UD optimizes on a token distribution, we follow their original initialization strategy by setting the first few tokens to be the target prompt, and initializing the rest of the tokens from a uniform distribution for all tokens. Without this type of initialization UD does not achieve any significant results. Each restoration method is evaluated by identifying 50 adversarial prompts on an H100 GPU and using which to generate 500 images per method for ASR calculations. For RECORD, we use $N = 20$ passes through the token list, a batch size of 1 image each, and $J = 64$ samples for the candidate selection. The chosen candidate set has size $K = 64$. Example images can be found in Table 1 and Appendix K.

RECORD consistently outperforms P4D and UD (Table 3) by up to 17.8 times (see the AdvUnlearn-Parachute cells), except for a few minor exceptions. In particular, AdvUnlearn is quite resilient against P4D and UD with single digit ASR on most concepts, while RECORD is able to achieve an ASR of at least 33% for all concepts. Additionally, different erasure methods seem to have different level of robustness against adversarial attacks on different concepts. For example, ED (Wu et al., 2024) is more robust in erasing nudity-related concepts, but not on objects such as church. Similar observation can also be observed in Appendix F. On the other hand, SH models are very robust against all concept restoration attacks, but this comes at a significant cost of the generation quality of other non-erased concepts, which has been discussed in detail by (Zhang et al., 2024b). We additionally conduct fixed-seed ablation study and demonstrate RECORD still perform well in Appendix E.

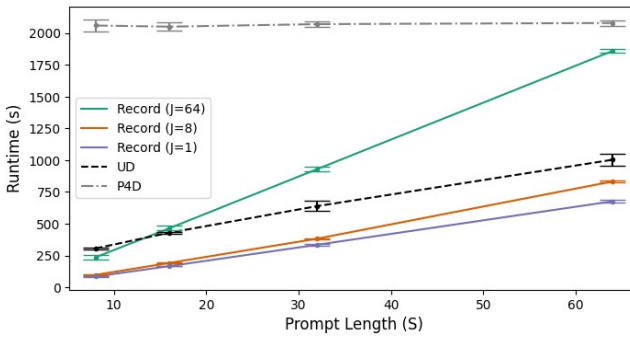


Figure 3: The mean runtime and the standard deviation (annotated as error bars) of different restoration methods, computed over 10 runs and at sequence lengths $S = 8, 16, 32, 64$. We note it is possible to achieve substantial acceleration by lowering gradient token number J , with only marginal performance loss, as discussed in Appendix D.

5 DISCUSSIONS

To validate the design of RECORD, we conducted several ablation studies. First, we addressed the ongoing debate in the literature regarding the optimal loss function for concept restoration (Pham et al., 2023; Zhang et al., 2023; Chin et al., 2023). Our findings in Appendix B show that the loss function in Equation [1], which uses the original model’s noise prediction as a target, marginally outperforms alternatives that rely on Gaussian noise. This is because the original model’s predictions act as a more informative surrogate, justifying its slight increase in computational overhead.

The runtime of RECORD is very competitive with existing restoration methods (Figure 3), and its hyperparameters S, N, J, K provide flexible control over the compute-performance trade-off (Appendices C,D). For example, our ablation studies in Appendix D demonstrate that a significant 60% acceleration can be achieved by lowering the number of gradient tokens J with only a marginal loss in performance. This allows RECORD’s runtime to surpass that of P4D and UD while maintaining its superior ASRs. Additionally, our studies on prompt length S and the number of passes N conclude that the best strategy for maximizing ASR for a given compute budget is to choose higher S and lower N , as the breath of the search space is more significant than the depth. These results can be found in Appendix C.

We also tested the transferability of successful adversarial prompts from SD1.4 to larger unlearned models like SDXL (Podell et al., 2024) and FLUX (Labs et al., 2025) in Appendix F. Our results show that adversarial prompts identified by RECORD are generally more transferable than those from P4D and UD. This finding has significant black-box implications, as an adversary could use a prompt optimized on an open-sourced model to attack a different black box model without requiring access to the model weights. This superior level of transferability allows RECORD to mitigate the limitations of the white-box assumption commonly used by the existing concept restoration methods.

Lastly, we investigate the scalability of RECORD on a more challenging setting i.e. restoring erased concepts on more sophisticated text-to-image models, such as SDXL and FLUX. In particular, these larger models have a dual-encoder setup for encoding prompts, which differs from the single text encoder used in SD1.4. This introduces additional difficulties in restoration algorithm design and is rarely addressed in the existing concept restoration literature (Zhang et al., 2025). We assess five different strategies for adapting RECORD to handle this architectural difference and provide some initial results (Appendix G). Example images by SDXL and FLUX are showcased in Appendix L.

6 CONCLUSIONS

In this study, our investigation into existing concept erasure methods used in text-to-image diffusion models reveal that adversarial prompt embeddings are pervasive throughout the embedding space, which can be exploited by token-level concept restoration methods. We further introduce RECORD, a novel token-level concept restoration algorithm designed for restoring erased concepts by adversarially perturbing the input prompts in a coordinate-descent manner. We conduct extensive experiments and ablation studies demonstrating the consistent superiority of RECORD as well as the effect of its hyperparameters. These results not only underscore significant vulnerability inherent in current erasure approaches, but also pave the way for the future development of erasure and restoration algorithms that can more effectively mitigate or exploit these vulnerabilities.

486 REFERENCES

487

488 P. Bedapudi. Nudenet: Neural nets for nudity classification, detection and selective censoring.
489 <https://github.com/notAI-tech/NudeNet>, 2019.

490 Lucas Beerens and Desmond J Higham. Adversarial ink: Componentwise backward error attacks on
491 deep learning. 89(1):175–196, 2024. ISSN 0272-4960. doi: 10.1093/imamat/hxad017.

492 Nicholas Carlini, Milad Nasr, Christopher A. Choquette-Choo, Matthew Jagielski, Irena Gao, Anas
493 Awadalla, Pang Wei Koh, Daphne Ippolito, Katherine Lee, Florian Tramer, and Ludwig Schmidt.
494 Are aligned neural networks adversarially aligned? In *NeurIPS*, 2023. doi: 10.48550/arXiv.2306.
495 15447.

496 Zhi-Yi Chin, Chieh-Ming Jiang, Ching-Chun Huang, Pin-Yu Chen, and Wei-Chen Chiu. Prompt-
497 ing4Debugging: Red-teaming text-to-image diffusion models by finding problematic prompts. In
498 *ICML*, September 2023. doi: 10.48550/arXiv.2309.06135.

499 Kevin Clark and Priyank Jaini. Text-to-image diffusion models are zero-shot classifiers. In *NeurIPS*,
500 March 2023. doi: 10.48550/arXiv.2303.15233.

501 Yinpeng Dong, Fangzhou Liao, Tianyu Pang, Hang Su, Jun Zhu, Xiaolin Hu, and Jianguo Li. Boosting
502 Adversarial Attacks with Momentum. 2018. doi: 10.48550/arXiv.1710.06081.

503 Alexey Dosovitskiy, Lucas Beyer, Alexander Kolesnikov, Dirk Weissenborn, Xiaohua Zhai, Thomas
504 Unterthiner, Mostafa Dehghani, Matthias Minderer, Georg Heigold, Sylvain Gelly, Jakob Uszkoreit,
505 and Neil Houlsby. An Image is Worth 16x16 Words: Transformers for Image Recognition at Scale.
506 October 2020.

507 Javid Ebrahimi, Anyi Rao, Daniel Lowd, and Dejing Dou. HotFlip: White-box adversarial examples
508 for text classification. (arXiv:1712.06751), May 2018. doi: 10.48550/arXiv.1712.06751.

509 Chongyu Fan, Jiancheng Liu, Yihua Zhang, Eric Wong, Dennis Wei, and Sijia Liu. SalUn: Em-
510 powering machine unlearning via gradient-based weight saliency in both image classification and
511 generation. In *ICLR*, October 2023. doi: 10.48550/arXiv.2310.12508.

512 Alhussein Fawzi, Hamza Fawzi, and Omar Fawzi. Adversarial vulnerability for any classifier. In
513 *Advances in Neural Information Processing Systems*, volume 31. Curran Associates, Inc., 2018.

514 Rinon Gal, Yuval Alaluf, Yuval Atzmon, Or Patashnik, Amit H. Bermano, Gal Chechik, and Daniel
515 Cohen-Or. An image is worth one word: Personalizing text-to-image generation using textual
516 inversion. In *ICLR*, August 2022. doi: 10.48550/arXiv.2208.01618.

517 Rohit Gandikota, Joanna Materzynska, Jaden Fiotto-Kaufman, and David Bau. Erasing concepts
518 from diffusion models. In *ICCV*, March 2023a. doi: 10.1109/ICCV51070.2023.00230.

519 Rohit Gandikota, Hadas Orgad, Yonatan Belinkov, Joanna Materzyńska, and David Bau. Unified
520 concept editing in diffusion models. In *IEEE Workshop/Winter Conference on Applications of
521 Computer Vision*, pp. 5099–5108. arXiv, August 2023b. doi: 10.1109/WACV57701.2024.00503.

522 Daiheng Gao, Shilin Lu, Shaw Walters, Wenbo Zhou, Jiaming Chu, Jie Zhang, Bang Zhang, Mengxi
523 Jia, Jian Zhao, Zhaoxin Fan, and Weiming Zhang. EraseAnything: Enabling Concept Erasure in
524 Rectified Flow Transformers. abs/2412.20413, 2024. ISSN 2331-8422. doi: 10.48550/arXiv.2412.
525 20413.

526 Chao Gong, Kai Chen, Zhipeng Wei, Jingjing Chen, and Yu-Gang Jiang. Reliable and Efficient
527 Concept Erasure of Text-to-Image Diffusion Models. In *ECCV*, July 2024. doi: 10.48550/arXiv.
528 2407.12383.

529 Chuan Guo, Alexandre Sablayrolles, Hervé Jégou, and Douwe Kiela. Gradient-based Adversarial
530 Attacks against Text Transformers. In *EMNLP*, 2021. doi: 10.18653/v1/2021.emnlp-main.464.

531 Xiaoxuan Han, Songlin Yang, Wei Wang, Yang Li, and Jing Dong. Probing unlearned diffusion
532 models: A transferable adversarial attack perspective. (arXiv:2404.19382), April 2024. doi:
533 10.48550/arXiv.2404.19382.

540 Anubhav Jain, Yuya Kobayashi, Takashi Shibuya, Yuhta Takida, Nasir Memon, Julian Togelius, and
541 Yuki Mitsufuji. TraSCE: Trajectory Steering for Concept Erasure. (arXiv:2412.07658), December
542 2024. doi: 10.48550/arXiv.2412.07658.

543

544 Eric Jang, Shixiang Gu, and Ben Poole. Categorical reparameterization with gumbel-softmax.
545 (arXiv:1611.01144), August 2017. doi: 10.48550/arXiv.1611.01144.

546 Erik Jones, Anca Dragan, Aditi Raghunathan, and Jacob Steinhardt. Automatically auditing large
547 language models via discrete optimization. In *ICML*, March 2023. doi: 10.48550/arXiv.2303.
548 04381.

549

550 Changhoon Kim and Yanjun Qi. A Comprehensive Survey on Concept Erasure in Text-to-Image
551 Diffusion Models. 2025. doi: 10.48550/arXiv.2502.14896.

552 Changhoon Kim, Kyle Min, and Yezhou Yang. R.A.C.E.: Robust Adversarial Concept Erasure for
553 Secure Text-to-Image Diffusion Model. In *ECCV*, May 2024. doi: 10.48550/arXiv.2405.16341.

554

555 Nupur Kumari, Bingliang Zhang, Sheng-Yu Wang, Eli Shechtman, Richard Zhang, and Jun-Yan
556 Zhu. Ablating concepts in text-to-image diffusion models. In *ICCV*, March 2023. doi: 10.1109/
557 ICCV51070.2023.02074.

558

559 Alexey Kurakin, Ian Goodfellow, and Samy Bengio. Adversarial examples in the physical world. In
560 *ICLR*, 2016. doi: 10.1201/9781351251389-8.

561

562 Black Forest Labs, Stephen Batifol, Andreas Blattmann, Frederic Boesel, Saksham Consul, Cyril
563 Diagne, Tim Dockhorn, Jack English, Zion English, Patrick Esser, Sumith Kulal, Kyle Lacey, Yam
564 Levi, Cheng Li, Dominik Lorenz, Jonas Müller, Dustin Podell, Robin Rombach, Harry Saini, Axel
565 Sauer, and Luke Smith. Flux.1 kontext: Flow matching for in-context image generation and editing
566 in latent space. 2025.

567

568 Alexander C. Li, Mihir Prabhudesai, Shivam Duggal, Ellis Brown, and Deepak Pathak. Your diffusion
569 model is secretly a zero-shot classifier. In *ICCV*, March 2023. doi: 10.1109/ICCV51070.2023.
570 00210.

571

572 Hang Li, Chengzhi Shen, Philip Torr, Volker Tresp, and Jindong Gu. Self-Discovering Interpretable
573 Diffusion Latent Directions for Responsible Text-to-Image Generation. In *CVPR*, March 2024.
574 doi: 10.1109/CVPR52733.2024.01141.

575

576 Junnan Li, Dongxu Li, Caiming Xiong, and Steven Hoi. BLIP: Bootstrapping language-image
577 pre-training for unified vision-language understanding and generation. In *ICML*, January 2022.
578 doi: 10.48550/arXiv.2201.12086.

579

580 Kevin Lu, Nicky Kriplani, Rohit Gandikota, Minh Pham, David Bau, Chinmay Hegde, and Niv
581 Cohen. When Are Concepts Erased From Diffusion Models? abs/2505.17013, 2025. ISSN
582 2331-8422. doi: 10.48550/arXiv.2505.17013.

583

584 Mengyao Lyu, Yuhong Yang, Haiwen Hong, Hui Chen, Xuan Jin, Yuan He, Hui Xue, Jungong Han,
585 and Guiguang Ding. One-dimensional adapter to rule them all: Concepts, diffusion models and
586 erasing applications. In *CVPR*, March 2024. doi: 10.1109/CVPR52733.2024.00722.

587

588 Minh Pham, Kelly O. Marshall, Niv Cohen, Govind Mittal, and Chinmay Hegde. Circumventing
589 concept erasure methods for text-to-image generative models. In *ICLR*, August 2023. doi:
590 10.48550/arXiv.2308.01508.

591

592 Dustin Podell, Zion English, Kyle Lacey, Andreas Blattmann, Tim Dockhorn, Jonas Müller, Joe
593 Penna, and Robin Rombach. Sdxl: Improving latent diffusion models for high-resolution image
synthesis. In B. Kim, Y. Yue, S. Chaudhuri, K. Fragniadi, M. Khan, and Y. Sun (eds.), *ICLR*,
volume 2024, pp. 1862–1874, 2024.

594

595 Alec Radford, Jong Wook Kim, Chris Hallacy, Aditya Ramesh, Gabriel Goh, Sandhini Agarwal,
596 Girish Sastry, Amanda Askell, Pamela Mishkin, Jack Clark, Gretchen Krueger, and Ilya Sutskever.
597 Learning transferable visual models from natural language supervision. In *ICML*, February 2021.
598 doi: 10.48550/arXiv.2103.00020.

594 Colin Raffel, Noam Shazeer, Adam Roberts, Katherine Lee, Sharan Narang, Michael Matena, Yanqi
595 Zhou, Wei Li, and Peter J. Liu. Exploring the limits of transfer learning with a unified text-to-text
596 transformer. *CoRR*, abs/1910.10683, 2019.

597 Joseph Redmon and Ali Farhadi. YOLOv3: An Incremental Improvement. (arXiv:1804.02767),
598 April 2018. doi: 10.48550/arXiv.1804.02767.

600 Robin Rombach, Andreas Blattmann, Dominik Lorenz, Patrick Esser, and Björn Ommer. High-
601 resolution image synthesis with latent diffusion models. (arXiv:2112.10752), April 2022. doi:
602 10.48550/arXiv.2112.10752.

603 Olaf Ronneberger, Philipp Fischer, and Thomas Brox. U-Net: Convolutional Networks for Biomedical
604 Image Segmentation. In Nassir Navab, Joachim Hornegger, William M. Wells, and Alejandro F.
605 Frangi (eds.), *Medical Image Computing and Computer-Assisted Intervention – MICCAI 2015*,
606 pp. 234–241, Cham, 2015. Springer International Publishing. ISBN 978-3-319-24574-4. doi:
607 10.1007/978-3-319-24574-4_28.

609 Patrick Schramowski, Manuel Brack, Björn Deisereth, and Kristian Kersting. Safe Latent Diffusion:
610 Mitigating Inappropriate Degeneration in Diffusion Models. In *CVPR*, April 2023. doi: 10.1109/
611 CVPR52729.2023.02157.

612 Weijia Shi, Xiaochuang Han, Hila Gonen, Ari Holtzman, Yulia Tsvetkov, and Luke Zettlemoyer.
613 Toward Human Readable Prompt Tuning: Kubrick’s The Shining is a good movie, and a good
614 prompt too? In *EMNLP*, December 2022. doi: 10.48550/arXiv.2212.10539.

616 Taylor Shin, Yasaman Razeghi, Robert L. Logan Iv, Eric Wallace, and Sameer Singh. AutoPrompt:
617 Eliciting Knowledge from Language Models with Automatically Generated Prompts. In *EMNLP*,
618 Online, 2020. doi: 10.18653/v1/2020.emnlp-main.346.

619 Carl-Johann Simon-Gabriel, Yann Ollivier, Léon Bottou, Bernhard Schölkopf, and David Lopez-
620 Paz. Adversarial Vulnerability of Neural Networks Increases With Input Dimension. *arXiv.org*,
621 abs/1802.01421, February 2018. ISSN 2331-8422. doi: 10.48550/arXiv.1802.01421.

623 Gowthami Somepalli, Vasu Singla, Micah Goldblum, Jonas Geiping, and Tom Goldstein. Diffusion
624 Art or Digital Forgery? Investigating Data Replication in Diffusion Models. In *CVPR*, December
625 2022. doi: 10.1109/CVPR52729.2023.00586.

626 Jiaming Song, Chenlin Meng, and Stefano Ermon. Denoising diffusion implicit models. In *ICLR*,
627 October 2020.

629 Koushik Srivatsan, Fahad Shamshad, Muzammal Naseer, Vishal M. Patel, and Karthik Nandakumar.
630 STEREO: A Two-Stage Framework for Adversarially Robust Concept Erasing from Text-to-Image
631 Diffusion Models. In *Computer Vision and Pattern Recognition*. arXiv, 2025. doi: 10.1109/
632 CVPR52734.2025.02213.

634 Yu-Lin Tsai, Chia-Yi Hsu, Chulin Xie, Chih-Hsun Lin, Jia-You Chen, Bo Li, Pin-Yu Chen, Chia-Mu
635 Yu, and Chun-Ying Huang. Ring-a-bell! How reliable are concept removal methods for diffusion
636 models? In *ICLR*, October 2023. doi: 10.48550/arXiv.2310.10012.

637 Eric Wallace, Shi Feng, Nikhil Kandpal, Matt Gardner, and Sameer Singh. Universal adversarial
638 triggers for attacking and analyzing NLP. (arXiv:1908.07125), January 2021. doi: 10.48550/arXiv.
639 1908.07125.

641 Jianzhong Wang. *Isomaps*, pp. 151–180. Springer Berlin Heidelberg, Berlin, Heidelberg, 2012. ISBN
642 978-3-642-27497-8. doi: 10.1007/978-3-642-27497-8_8.

643 Yuxin Wen, Neel Jain, John Kirchenbauer, Micah Goldblum, Jonas Geiping, and Tom Goldstein.
644 Hard prompts made easy: Gradient-based discrete optimization for prompt tuning and discovery.
645 In *NeurIPS*, February 2023. doi: 10.48550/arXiv.2302.03668.

647 Jing Wu and Mehrtash Harandi. Scissorhands: Scrub data influence via connection sensitivity in
648 networks. In *ECCV*, January 2024. doi: 10.48550/arXiv.2401.06187.

648 Jing Wu, Trung Le, Munawar Hayat, and Mehrtash Harandi. EraseDiff: Erasing data influence in
649 diffusion models. (arXiv:2401.05779), July 2024.
650

651 Kaiwen Wu, Allen Wang, and Yaoliang Yu. Stronger and Faster Wasserstein Adversarial Attacks. In
652 *ICML*, November 2020.

653 Yijun Yang, Ruiyuan Gao, Xiaosen Wang, Tsung-Yi Ho, Nan Xu, and Qiang Xu. MMA-Diffusion:
654 MultiModal Attack on Diffusion Models. In *Computer Vision and Pattern Recognition*. arXiv,
655 2024. doi: 10.1109/CVPR52733.2024.00739.

656

657 Jaehong Yoon, Shoubin Yu, Vaidehi Patil, Huaxiu Yao, and Mohit Bansal. SAFREE: Training-Free
658 and Adaptive Guard for Safe Text-to-Image And Video Generation. In *ICLR*, October 2024. doi:
659 10.48550/arXiv.2410.12761.

660 Gong Zhang, Kai Wang, Xingqian Xu, Zhangyang Wang, and Humphrey Shi. Forget-me-not:
661 Learning to forget in text-to-image diffusion models. In *CVPR*, Seattle, WA, USA, June 2024a.
662 ISBN 979-8-3503-6547-4. doi: 10.1109/CVPRW63382.2024.00182.

663

664 Yang Zhang, Er Jin, Yanfei Dong, Yixuan Wu, Philip Torr, Ashkan Khakzar, Johannes Stegmaier,
665 and Kenji Kawaguchi. Minimalist Concept Erasure in Generative Models. *abs/2507.13386*, 2025.
666 ISSN 2331-8422. doi: 10.48550/arXiv.2507.13386.

667 Yimeng Zhang, Jinghan Jia, Xin Chen, Aochuan Chen, Yihua Zhang, Jiancheng Liu, Ke Ding, and
668 Sijia Liu. To generate or not? Safety-driven unlearned diffusion models are still easy to generate
669 unsafe images ... For now. In *ECCV*, October 2023. doi: 10.48550/arXiv.2310.11868.

670 Yimeng Zhang, Xin Chen, Jinghan Jia, Yihua Zhang, Chongyu Fan, Jiancheng Liu, Mingyi Hong,
671 Ke Ding, and Sijia Liu. Defensive unlearning with adversarial training for robust concept erasure
672 in diffusion models. (arXiv:2405.15234), May 2024b. doi: 10.48550/arXiv.2405.15234.

673

674 Andy Zou, Zifan Wang, Nicholas Carlini, Milad Nasr, J. Zico Kolter, and Matt Fredrikson. Universal
675 and Transferable Adversarial Attacks on Aligned Language Models. *abs/2307.15043*, 2023. ISSN
676 2331-8422. doi: 10.48550/arXiv.2307.15043.

677

678

679

680

681

682

683

684

685

686

687

688

689

690

691

692

693

694

695

696

697

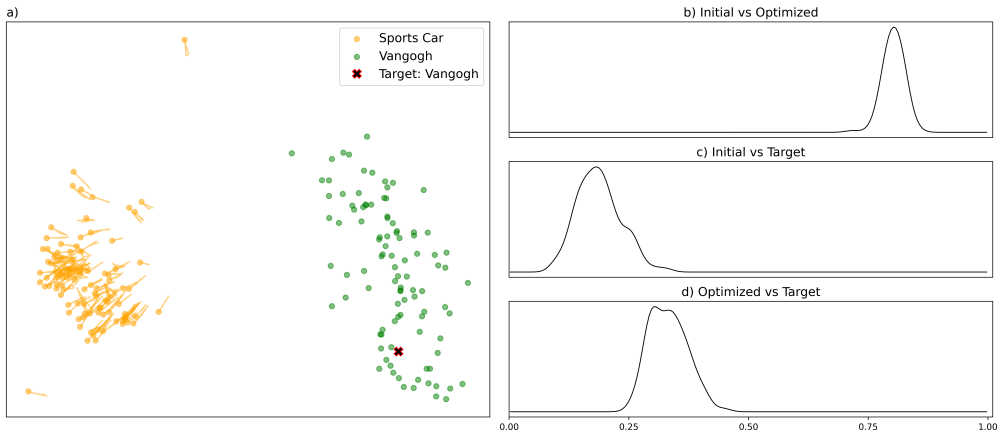
698

699

700

701

702 A "VULNERABILITY" ANALYSIS ON THE ORIGINAL MODEL



719
720 Figure 4: Behavior of the text embeddings during embedding-level attacks on original model. **a)**
721 Isomap projection of the optimization trajectories of the prompt embeddings. Dots denote the starting
722 point of the trajectory. The target concept can be generated at the end of each trajectory. **b), c), d)** are
723 smoothed cosine similarity histograms between the initial, optimized, and target embeddings.

724 Extending the discussion from Section 3.2, which established the pervasive existence of adversarial
725 embeddings in unlearned models, this section investigates the fundamental origin of this vulnerability.
726 We seek to answer a critical question: are these vulnerabilities an artifact of the concept erasure
727 process, or are they an intrinsic property of the original, pre-unlearned diffusion model?

728 To explore this, we conduct an experiment on the original, pre-unlearned model using the same
729 embedding-level optimization methodology described in Section 3.2. The objective is to determine if
730 prompt embeddings capable of generating a specific target concept could be discovered starting from
731 a completely irrelevant and semantically distant initial concept.

732 We use "a painting in the style of van Gogh" as the target prompt, and "a photorealistic image of a
733 sports car" as the semantically distant starting point. We generate 100 paraphrases of the starting
734 prompt and target prompt using Gemini 2.5 and encode them as the embedding initializations and as
735 the reference cluster, respectively.

736 Our findings reveal that even when initialized with embeddings for a "sports car," the optimization
737 process consistently discovers local embeddings that can generate van Gogh style paintings, far from
738 the region associated with the actual "van Gogh" prompt (Figure 4).

739 This result provides a crucial insight: the high-dimensional embedding space of the original model is
740 densely populated with regions that can trigger the generation of a given concept. The vulnerability to
741 concept restoration is therefore not primarily induced by the unlearning process but is an characteristic
742 inherited from the pre-unlearned model. Most concept erasure techniques focus on suppressing a
743 concept in the localized region around its explicit text description, leaving these numerous, distant
744 regions of vulnerabilities adversarially exploitable by the restoration attacks analyzed in this paper.

746
747
748
749
750
751
752
753
754
755

B EMBEDDING-LEVEL ATTACK RESULTS AND LOSS FUNCTION COMPARISON

Erased Concept	Restoration Method	Erasure Method					
		ESD 2023a	FMN 2024a	AC 2023	SPM 2024	UCE 2023b	AdvUnlearn 2024b
van Gogh	No attack	3.4	17.6	32.2	45.4	52.8	0.8
	Embed attack 1	99.8	99.8	99.4	100.0	91.4	92.8
	Embed attack 2	99.8	99.8	100.0	99.4	98.4	99.0
Erased Concept	Restoration Method	Erasure Method					
		ESD 2023a	ED 2024	SH 2024	SPM 2024	SalUn 2023	AdvUnlearn 2024b
Church	No attack	20.2	4.4	1.0	84.6	2.0	1.6
	Embed attack 1	95.6	99.4	22.8	98.0	99.4	96.6
	Embed attack 2	100.0	100.0	64.6	99.8	100.0	100.0
Garbage Truck	No attack	6.2	20.4	9.2	28.4	9.0	0.2
	Embed attack 1	98.0	98.4	18.0	98.0	99.6	96.2
	Embed attack 2	98.8	100.0	3.8	99.6	100.0	92.4
Parachute	No attack	0.8	3.8	2.2	29.8	1.2	0.2
	Embed attack 1	91.2	89.6	4.8	73.6	63.0	46.6
	Embed attack 2	99.4	93.8	1.2	46.6	61.6	44.8
Erased Concept	Restoration Method	Erasure Method					
		ESD 2023a	SH 2024	SPM 2024	SalUn 2023	UCE 2023b	AdvUnlearn 2024b
Nudity	No attack	49.2	2.0	49.6	1.8	41.8	38.4
	Embed attack 1	98.4	83.0	99.6	99.4	96.8	98.6
	Embed attack 2	98.2	87.6	98.6	99.8	98.8	96.8

Table 4: Attack success rate (%) of the embedding-level attacks for art style, object and nudity attacks. Embed attack 1 and 2 refer to the two loss formulation \tilde{L}_1 and \tilde{L}_2 , respectively.

The selection of an optimal loss function for identifying adversarial prompts to restore concepts from unlearned models is a topic of active debate (Pham et al., 2023; Zhang et al., 2023; Chin et al., 2023). This ablation study seeks to resolve this ambiguity by empirically comparing two prominent loss functions:

$$L_1(y) = \mathbb{E}_{t,z} \left[\left\| \epsilon_{\theta'}(z_t, t, \mathcal{T}(y)) - \epsilon \right\|_2^2 \right] \quad (3)$$

$$L_2(y) = \mathbb{E}_{t,z} \left[\left\| \epsilon_{\theta'}(z_t, t, \mathcal{T}(y)) - \epsilon_{\theta}(z_t, t, \mathcal{T}(y_{\text{target}})) \right\|_2^2 \right] \quad (4)$$

where z_t is obtained through the forward diffusion process, $z_0 \sim p_{\text{target}}$ is sampled from the target data distribution, y_{target} is the target prompt. L_1 (Pham et al., 2023) and L_2 (Chin et al., 2023) are minimized by optimizing prompts y to match the denoiser predictions respectively to: the true noise from the forward diffusion sequence ϵ , or the predicted noise by the baseline denoiser with the target prompt $\epsilon_\theta(z_t, t, \mathcal{T}(y_{\text{target}}))$.

To compare both loss functions, we consider the embedding-level attack setting:

$$\tilde{J}_1(c) \equiv \mathbb{E}_{t, z} \|\epsilon_{\theta'}(z_t, t, c) - \epsilon\|_2^2 \quad (5)$$

$$\tilde{L}_2(c) \equiv \mathbb{E}_{t, z} \left\| \epsilon_{\theta'}(z_t, t, c) - \epsilon_{\theta}(z_t, t, c_{\text{target}}) \right\|_2^2. \quad (6)$$

We use NAdam optimizer and iterate over a sampled z_0 set of 100 images 50 times, with a constant learning rate of 0.1 and a batch size of 16. z_0 is generated by the baseline model using the target

810 prompt. Attacks with each loss formulation find 500 adversarial prompt embeddings from random
811 initializations, and generate one image per prompt embedding to be classified in the same setting
812 described in Section 4.1.

813 The results are presented in Table 4. We notice that, for concepts where the classifier has a high
814 accuracy in classifying the images from the baseline model, as previously shown in Table 2, the
815 \tilde{L}_2 formulation performs marginally better than \tilde{L}_1 . For concepts whose classification accuracy
816 is already low on the baseline model, the difference between the two loss formulations becomes
817 negligible. This suggests when the baseline model can generate more ‘accurate’ images as perceived
818 by the classifier, the outputs of its denoiser can also act as a more informative surrogate to aid the
819 concept restoration process.

820 The RECORD algorithm discussed in this paper uses loss Equation [4] by default due to its marginal
821 improvement in the attack performance. Consequently, this particular loss may result in the increased
822 runtime of the RECORD algorithm, as well as requiring access to the baseline model ϵ_θ . These
823 limitations, however, can be mitigated or avoided by switching to loss Equation [3] at the expense of
824 a marginally poorer performance.

825
826
827
828
829
830
831
832
833
834
835
836
837
838
839
840
841
842
843
844
845
846
847
848
849
850
851
852
853
854
855
856
857
858
859
860
861
862
863

864 C ABLATION STUDY ON TOKENS LENGTHS
865
866
867
868
869

Erased Concept	Prompt Length S	Erasure Method					
		ESD 2023a	FMN 2024a	AC 2023	SPM 2024	UCE 2023b	AdvUnlearn 2024b
van Gogh	16	26.2	53.8	89.6	85.6	94.2	13.6
	32	40.0	69.6	92.4	91.8	95.4	29.4
	64	64.0	76.8	94.0	95.6	97.6	33.0
Erased Concept	Prompt Length S	Erasure Method					
		ED 2024	ESD 2023a	SalUn 2023	SH 2024	SPM 2024	AdvUnlearn 2024b
Church	16	34.8	58.0	52.8	4.6	89.4	42.4
	32	43.6	67.0	66.6	5.4	94.8	55.6
	64	61.2	75.2	71.4	8.6	92.2	57.0
Garbage Truck	16	18.8	26.2	43.0	1.6	69.0	63.8
	32	34.0	33.8	60.4	1.0	72.0	59.6
	64	40.8	38.8	58.0	1.0	66.4	50.0
Parachute	16	6.0	31.0	32.8	2.0	45.8	17.2
	32	10.0	36.6	35.4	1.0	55.8	26.2
	64	15.4	44.6	48.8	2.0	60.4	35.6
Nudity	16	3.6	62.2	5.2	23.6	54.8	48.4
	32	2.2	65.0	6.6	22.0	65.8	51.6
	64	2.4	70.6	9.0	21.2	69.0	39.2

891 Table 5: Attack success rate (%) of RECORD with different prompt length S .
892
893

Number of Passes N	Erasure Method			Number of Passes N	Prompt Length S	Erasure Method		
	ESD 2023a	AC 2023	AdvUnlearn 2024b			ESD 2023a	AC 2023	AdvUnlearn 2024b
5	50.8	91.0	7.8	80	16	33.6	91.4	30.4
10	58.4	92.4	28.2	40	32	45.8	91.2	33.8
15	65.8	93.6	22.0	20	64	64.0	94.0	33.0
20	64.0	94.0	33.0					

902 Table 6: Attack success rate (%) of RECORD with different number of passes N (left) and with fixed
903 number of optimization steps (right) on models unlearned on van Gogh style.
904
905

906 This section presents an ablation study to examine the effect of two key parameters of RECORD:
907 the number of tokens available for perturbation S and number of passes on the token sequence N .
908 The product of these two parameters, $N \times S$, corresponds to the total number of optimization steps,
909 which linearly scales the algorithm’s runtime. The rest of the parameter configuration is consistent
910 with that of Section 4.2.

911 Tables 5 and 6 demonstrate a strong impact of both N and S on RECORD’s performance. As
912 expected, increasing these parameters generally leads to better performance. However, a notable
913 finding is that even with $S = 16$, RECORD still achieves decent ASRs that often surpass those of
914 P4D and UD with $S = 64$ in Table 3. For $S = 16$, RECORD also has a much shorter runtime as
915 shown in Figure 3.

916 We also observed that reducing S has a more pronounced negative effect on ASR than reducing
917 N . This is evident in Table 6 (right), where a configuration with a smaller S but a compensating
918 increase in N , for maintaining a consistent total number of optimization steps, still resulted in a
919
920

918 decay in ASR. This decay, however, was less severe than a simple reduction in S in Table 5 without a
919 compensatory increase in N . This suggests the breadth of the search space of the adversarial tokens
920 is more critical than the depth of the search, and choosing a larger S is the preferred strategy for
921 maximizing performance for the same compute cost.

923 D ABLATION STUDY ON GRADIENT AND CANDIDATE TOKENS

926 927 928 929 930 931 932 933 934 935 936 937 938 939 940 941 942 943 944 945 946 947 948 949 950 951 952 953 954 955 956 957 958 959 960 961 962 963 964 965 966 967 968 969 970 971	926 927 928 929 930 931 932 933 934 935 936 937 938 939 940 941 942 943 944 945 946 947 948 949 950 951 952 953 954 955 956 957 958 959 960 961 962 963 964 965 966 967 968 969 970 971		
	926 927 928 929 930 931 932 933 934 935 936 937 938 939 940 941 942 943 944 945 946 947 948 949 950 951 952 953 954 955 956 957 958 959 960 961 962 963 964 965 966 967 968 969 970 971		
	926 927 928 929 930 931 932 933 934 935 936 937 938 939 940 941 942 943 944 945 946 947 948 949 950 951 952 953 954 955 956 957 958 959 960 961 962 963 964 965 966 967 968 969 970 971	926 927 928 929 930 931 932 933 934 935 936 937 938 939 940 941 942 943 944 945 946 947 948 949 950 951 952 953 954 955 956 957 958 959 960 961 962 963 964 965 966 967 968 969 970 971	926 927 928 929 930 931 932 933 934 935 936 937 938 939 940 941 942 943 944 945 946 947 948 949 950 951 952 953 954 955 956 957 958 959 960 961 962 963 964 965 966 967 968 969 970 971
Gradient Token J	ESD 2023a	AC 2023	AdvUnlearn 2024b
1	60.2	93.8	16.4
8	61.4	94.6	30.2
16	64.0	92.2	30.0
32	65.2	92.8	30.6
64	64.0	94.0	33.0
Candidate Token K	ESD 2023a	AC 2023	AdvUnlearn 2024b
1	17.4	65.8	2.4
8	54.6	93.0	8.4
16	54.2	90.4	17.8
32	61.2	95.2	29.8
64	64.0	94.0	33.0

Table 7: Combined tables showing van Gogh Gradient and Candidate Tokens.

Prompt Length S	Restoration Method Runtime/s			
	P4D	UD	RECORD (J=64)	RECORD (J=8)
8	2059±49	305±7	235±16	97±2
16	2050±34	429±7	464±18	191±2
32	2070±22	638±39	929±16	382±5
64	2079±22	1003±50	1859±15	832±7

Table 8: The mean and the standard deviation of the restoration method runtime are computed over 10 runs.

In this section, we conduct ablation studies on the gradient token number J and candidate token number K to justify the design choices as well as the performance and efficiency of the RECORD algorithm. The rest of the experimental setting is consistent to that of Section 4.2.

Our experiments demonstrate that increasing the number of gradient tokens J , which are used for linearised gradient estimation, yields only marginal performance improvements in terms of ASRs. In contrast, the number of candidate tokens K for exact evaluation has a more significant impact on boosting ASRs.

This finding suggests it is possible to substantially accelerate the algorithm by significantly reducing J to accelerate the algorithm. Notably, with $J = 8$, the runtime of the algorithm can be reduced by 60%, while having only a marginal relative drop in ASRs of 5 – 10%, or 3 – 4% in absolute terms. Smaller J also helps in reducing memory consumption, as gradient estimation through backpropagation with J tokens corresponds to a major but now mitigable memory bottleneck.

972
973
974
975

E FIXED SEED ATTACKS

976
977
978
979
980
981

Erased Concept	Restoration Method	Erasure Method					
		ED 2024	ESD 2023a	SalUn 2023	SH 2024	SPM 2024	AdvUnlearn 2024b
Nudity	P4D 2023	3.4	84.8	21.2	4.2	100.0	27.1
	UD 2023	1.7	87.3	19.5	11.0	100.0	22.0
	RECORD	1.7	98.3	30.5	9.3	100.0	41.5

982
983
984
985
986
987
988
989
990
991
992
993
994
995
996
997
998
999
1000
1001
1002
1003
1004
1005
1006
1007
1008
1009
1010
1011
1012
1013
1014
1015
1016
1017
1018
1019
1020
1021
1022
1023
1024
1025

Table 9: Attack success rate (%) of concept restoration methods in the fixed-seed setting.

To assess the performance of RECORD in the fixed-seed setting, we follow the experimental setup of UD (Zhang et al., 2023), where the target prompt-seed pairs are taken from the I2P dataset (Schramowski et al., 2023), which fixes the generation seed. In these experiments, we also similarly follow the previous works of using a NudeNet classifier (Bedapudi, 2019) and evaluates the optimized prompts on-the-fly: if a generated image is deemed unsafe, the optimization stops immediately.

Under this setting, we note RECORD achieves highly competitive performance in comparison with P4D and UD, especially on concept-erased models that are easier to attack, such as ESD, SalUn, and AdvUnlearn.

1026 F ADVERSARIAL PROMPT TRANSFERABILITY

1028 This section investigates the transferability of adversarial prompts generated by different concept
 1029 erasure and restoration methods. Specifically, we examine whether prompts optimized on an unlearned
 1030 SD1.4 model can successfully generate erased concepts on other models, such as SDXL and FLUX
 1031 unlearned using ESD. This study assesses the generalizability and robustness of these prompts across
 1032 different model architectures and explores the feasibility for an external adversary to use prompts
 1033 optimized on a white-box open-source model to attack a different black-box model.

1034 Our analysis uses a collection of adversarial prompts that can successfully generate erased concepts
 1035 on their correspondingly unlearned SD1.4 models. Any prompts that fail to generate the erased
 1036 concepts are not included in this study. As shown in Table 10, the adversarial prompts identified
 1037 by the RECORD method exhibit greater transferability than those from P4D and UD, often by a
 1038 significant margin. This suggests that the optimization strategy of RECORD produces prompts that
 1039 are more robust and less model-specific.

1040 We also observed that prompt transferability is highly dependent on both the specific erased concept
 1041 and the target model. Adversarial prompts from SD1.4 generally transferred better to SDXL than
 1042 to FLUX. This is likely due to the significant differences in training data and model architecture
 1043 between SD1.4 and FLUX. Despite these differences, it is interesting to note that some level of
 1044 transferability can still be preserved. This suggests a fundamental, underlying transferability of
 1045 adversarial prompts in general, indicating that they retain some semantic meaning even when they
 1046 appear as human-unreadable, gibberish-like strings.

1048 Erased 1049 Concept	1050 Model	1051 ESD			1052 AC			1053 AdvUnlearn		
		1054 P4D	1055 UD	1056 RECORD	1057 P4D	1058 UD	1059 RECORD	1060 P4D	1061 UD	1062 RECORD
1051 van 1052 Gogh	SDXL	2.0	4.0	5.0	4.4	3.8	6.0	1.6	3.4	10.8
	FLUX	0.2	0.0	1.4	0.0	0.4	1.8	0.8	0.2	2.4
1053 Erased 1054 Concept	1055 Model	1056 ESD			1057 SH			1058 AdvUnlearn		
		1059 P4D	1060 UD	1061 RECORD	1062 P4D	1063 UD	1064 RECORD	1065 P4D	1066 UD	1067 RECORD
1056 Church	SDXL	64.4	58.6	79.8	32.0	52.6	59.8	49.2	64.6	61.6
	FLUX	5.2	2.6	14.8	6.2	0.2	8.4	1.0	1.0	5.4
1059 Garbage 1060 Truck	SDXL	85.0	75.2	89.4	25.0	32.6	21.2	55.6	51.4	64.8
	FLUX	0.0	0.0	0.8	0.0	0.0	0.2	0.0	0.4	0.0
1062 Parachute	SDXL	56.2	55.2	63.4	2.6	21.6	23.0	23.8	37.4	46.4
	FLUX	0.0	0.0	0.0	0.2	0.0	0.0	0.0	0.0	0.0
1064 Nudity	SDXL	61.8	68.0	77.6	11.8	75.4	22.0	49.8	74.2	66.0
	FLUX	18.0	18.4	38.0	5.4	16.4	9.6	8.2	11.6	22.4

1067 Table 10: Attack success rate (%) of using successful adversarial prompts on SD1.4 on ESD-unlearned
 1068 SDXL and FLUX.

1069
 1070
 1071
 1072
 1073
 1074
 1075
 1076
 1077
 1078
 1079

G SCALABILITY ON LARGE MODELS

Candidate Selection Strategy	Erased Concepts			Average
	van Gogh	Church	Nudity	
Random switching	17.4	86.0	23.6	32.5
Interleaving	26.6	92.4	17.6	34.8
Blend $\alpha = 0.0$	19.0	92.4	26.6	35.4
Blend $\alpha = 0.5$	14.2	91.0	17.6	31.4
Blend $\alpha = 1.0$	7.2	89.2	15.0	28.4

Table 11: Attack success rate (%) of different candidate selection strategy for SDXL.

Candidate Selection Strategy	Erased Concepts			Average
	van Gogh	Church	Nudity	
Random switching	1.6	19.8	8.2	9.8
Blend $\alpha = 0.0$	5.0	54.6	14.4	24.7
Blend $\alpha = 1.0$	2.6	0.2	1.4	1.4

Table 12: Attack success rate (%) of different candidate selection strategy for FLUX.

We extend RECORD to work on larger models, namely SDXL (Podell et al., 2024) and FLUX (Labs et al., 2025). The major challenge is that SDXL and FLUX both use two separate text encoders for encoding input texts. This differs from SD1.4, where only one text encoder is used in its pipeline. This dual-encoder setup leads to difficulties in the candidate selection stage. For SDXL, both CLIP text encoders share a similar tokenizer with consistent token_id mapping, but with different embedding tables E_1 , E_2 and different CLIP encoders. In this case, we propose three different strategies for handling candidate selection:

- **Random Switching:** At each optimization step, randomly choose one of the two text encoders for computing score and select the top- K tokens.

$\mathcal{V} = \text{Top}_K(E_i g_i)$, where $i \sim \text{Uniform}\{1, 2\}$,

where g_i is the gradient of the corresponding embedding table E_i

- **Interleaving:** Compute two separate scores and select the top- $K/2$ tokens with respect to each text encoder. In our experience, the number of overlapping candidate tokens are negligible compared to the size of K .

$$\mathcal{V} = \text{Top}_{K/2}(E_1 g_1) \cup \text{Top}_{K/2}(E_2 g_2).$$

- **Blend**: Compute a mixture of the scores from both text encoders and select the top- K tokens.

$$\mathcal{V} = \text{Top}_K \left((1 - \alpha) E_1 g_1 + \alpha E_2 g_2 \right),$$

where $\alpha \in [0, 1]$ is a tunable hyperparameter. When $\alpha = 0$ or 1 , this is equivalent to optimizing over only one text encoder.

We denote the embedding tables of CLIP-ViT/L (CLIPTextModel) and CLIP-ViT/G (CLIPTextModelWithProjection) as E_1 and E_2 , respectively. The ASRs of the three strategies are presented in Table 11. We note that, for SDXL, using interleaving strategy or optimizing only on CLIP-ViT/L works the best. Example images can be found in Appendix L.

FLUX uses CLIP and T5 (Raffel et al., 2019) as its text encoders with two completely different tokenizers. Tokens of the two text encoders thus correspond to different strings of text. This is exacerbated by the non-bijective nature of the token-string mappings, i.e. original token \rightarrow string \rightarrow token \neq original token. These make Interleaving and Blend not applicable, unless $\alpha \in \{0, 1\}$. Here we consider the embedding tables of CLIP and T5 encoder as E_1 and E_2 . RECORD performs best on FLUX when only optimizing on the CLIP encoder (Table 12), which is mostly consistent with the behavior in SDXL.

H EXPERIMENTS ON ADDITIONAL CONCEPTS AND CONCEPT ERASURE METHODS

In this section, we further expand the evaluation scope of our study to cover six additional concepts (tench, car, french horn, violence, illegal activity, Barack Obama) on two more concept erasure methods (SAFREE (Yoon et al., 2024), STEREO (Srivatsan et al., 2025)). The results continue to demonstrate the significantly superior performance of RECORD over other attack baselines.

Erased Concept	Restoration Method	Erasure Method			
		ESD 2023a	AdvUnlearn 2024b	SAFREE 2024	STEREO 2025
Car	P4D 2023	26.6	2.8	6.8	2.2
	UD 2023	8.6	0.1	2.6	2.6
	RECORD	53.8	60.2	63.0	4.0
French Horn	P4D 2023	17.4	5.8	0.8	0.4
	UD 2023	2.3	0.0	0.0	0.4
	RECORD	70.6	87.8	94.0	1.0
Violence	P4D 2023	28.6	7.6	25.8	7.0
	UD 2023	37.8	10.9	11.8	13.2
	RECORD	67.2	57.2	73.0	14.6
Drugs	P4D 2023	45.6	12.8	8.2	5.4
	UD 2023	7.6	3.3	8.6	4.0
	RECORD	87.6	89.0	88.0	21.2
Obama	P4D 2023	6.6	1.8	0.6	0.4
	UD 2023	2.6	2.3	1.6	0.0
	RECORD	30.8	15.6	98.6	3.2
Tench	P4D 2023	39.8	0.6	0.6	0.0
	UD 2023	4.5	27.3	1.0	0.4
	RECORD	79.0	71.8	85.6	1.2

Table 13: Attack success rate (%) of additional concepts and concept erasure methods on SD1.4.

1188
1189

I LLM USAGE DECLARATION

1190
1191
1192

Large language models have been occasionally used in this project for polishing writing, suggesting and applying bug fixes with significant human oversight, and for interfacing with computing infrastructure such as Slurm and Kubernetes.

1193
1194

J EMBEDDING-LEVEL ATTACK EXAMPLE IMAGES

1196
1197
1198

In this section we present SD1.4 example images generated by different restoration methods, as well as from the embedding-level attack discussion in Appendix B

1200 1201 1202 1203 1204 1205 1206 1207 1208 1209 1210 1211 1212 1213 1214	1200 1201 1202 1203 1204 1205 1206 1207 1208 1209 1210 1211 1212 1213 1214	1200 1201 1202 1203 1204 1205 1206 1207 1208 1209 1210 1211 1212 1213 1214	1200 1201 1202 1203 1204 1205 1206 1207 1208 1209 1210 1211 1212 1213 1214						
1200 1201 1202 1203 1204 1205 1206 1207 1208 1209 1210 1211 1212 1213 1214	1200 1201 1202 1203 1204 1205 1206 1207 1208 1209 1210 1211 1212 1213 1214	1200 1201 1202 1203 1204 1205 1206 1207 1208 1209 1210 1211 1212 1213 1214	Erasure Method	ESD 2023a	FMN 2024a	AC 2023	SPM 2024	UCE 2023b	AdvUnlearn 2024b
1215 1216 1217 1218 1219	1215 1216 1217 1218 1219	1215 1216 1217 1218 1219	No attack						
1220 1221 1222	1220 1221 1222	1220 1221 1222	van Gogh						
1223 1224 1225 1226 1227 1228 1229 1230 1231 1232 1233 1234	1223 1224 1225 1226 1227 1228 1229 1230 1231 1232 1233 1234	1223 1224 1225 1226 1227 1228 1229 1230 1231 1232 1233 1234	Embed attack 1						
1235 1236 1237 1238 1239 1240 1241	1235 1236 1237 1238 1239 1240 1241	1235 1236 1237 1238 1239 1240 1241	Embed attack 2						

Table 14: Generated images of erased concepts using embedding-level attacks. Each image column of the same concept is generated using the same latent initialization. Models have unlearned the style of van Gogh paintings. Target prompt "a painting in the style of van Gogh"

1220 1221 1222 1223 1224 1225 1226 1227 1228 1229 1230 1231 1232 1233 1234	1220 1221 1222 1223 1224 1225 1226 1227 1228 1229 1230 1231 1232 1233 1234	1220 1221 1222 1223 1224 1225 1226 1227 1228 1229 1230 1231 1232 1233 1234	1220 1221 1222 1223 1224 1225 1226 1227 1228 1229 1230 1231 1232 1233 1234						
1220 1221 1222 1223 1224 1225 1226 1227 1228 1229 1230 1231 1232 1233 1234	1220 1221 1222 1223 1224 1225 1226 1227 1228 1229 1230 1231 1232 1233 1234	1220 1221 1222 1223 1224 1225 1226 1227 1228 1229 1230 1231 1232 1233 1234	No attack						
1235 1236 1237 1238 1239 1240 1241	1235 1236 1237 1238 1239 1240 1241	1235 1236 1237 1238 1239 1240 1241	Embed attack 1						
1235 1236 1237 1238 1239 1240 1241	1235 1236 1237 1238 1239 1240 1241	1235 1236 1237 1238 1239 1240 1241	Embed attack 2						

Table 15: Generated images of erased concepts using embedding-level attacks. Each image column of the same concept is generated using the same latent initialization. Models have unlearned the concept of nudity. Target prompt asked for nudity.

1242 **K TOKEN-LEVEL ATTACK EXAMPLE IMAGES**
1243
1244
1245
1246
1247

Erased Concept	Restoration Method	Erasure Method					
		ESD 2023a	ED 2024	SH 2024	SPM 2024	SalUn 2023	AdvUnlearn 2024b
Church	No attack						
	Embed attack 1						
	Embed attack 2						
Garbage Truck	No attack						
	Embed attack 1						
	Embed attack 2						
Parachute	No attack						
	Embed attack 1						
	Embed attack 2						

1272
1273
1274
1275
1276
1277
1278
1279
1280
1281
1282
1283
1284
1285
1286
1287
1288
1289
1290
1291
1292
1293
1294
1295

Table 16: The generated images of erased concepts using embedding-level attacks. Each image column of the same concept is generated using the same latent initialization. Target prompt "a photorealistic image of {object}"

1296
1297
1298
1299
1300
1301

1302 1303 1304 1305 1306 1307 1308 1309 1310 1311 1312 1313 1314 1315 1316	1302 1303 1304 1305 1306 1307 1308 1309 1310 1311 1312 1313 1314 1315 1316	1302 1303 1304 1305 1306 1307 1308 1309 1310 1311 1312 1313 1314 1315 1316	Erasure Method						
1302 1303 1304 1305 1306 1307 1308 1309 1310 1311 1312 1313 1314 1315 1316									
1302 1303 1304 1305 1306 1307 1308 1309 1310 1311 1312 1313 1314 1315 1316	1302 1303 1304 1305 1306 1307 1308 1309 1310 1311 1312 1313 1314 1315 1316	1302 1303 1304 1305 1306 1307 1308 1309 1310 1311 1312 1313 1314 1315 1316	P4D 2023						
			UD 2023						
			RECORD						
1317 1318 1319 1320 1321 1322 1323 1324 1325 1326 1327 1328	1317 1318 1319 1320 1321 1322 1323 1324 1325 1326 1327 1328	1317 1318 1319 1320 1321 1322 1323 1324 1325 1326 1327 1328	P4D 2023						
			UD 2023						
			RECORD						
1329 1330 1331 1332 1333 1334 1335 1336 1337 1338 1339 1340	1329 1330 1331 1332 1333 1334 1335 1336 1337 1338 1339 1340	1329 1330 1331 1332 1333 1334 1335 1336 1337 1338 1339 1340	P4D 2023						
			UD 2023						
			RECORD						

1341
1342 Table 17: The generated images of erased concepts using token-level attacks. Each image column of
1343 the same concept is generated using the same latent initialization. Target prompt "a photorealistic
1344 image of {object}"

1345
1346
1347
1348
1349

1350
1351
1352
1353
1354
1355
1356
1357
1358
1359
1360
1361
1362
1363
1364
1365
1366
1367
1368
1369
1370
1371
1372
1373
1374
1375
1376
1377
1378
1379
1380
1381
1382
1383
1384
1385
1386
1387
1388
1389
1390
1391
1392
1393
1394
1395
1396
1397
1398
1399
1400
1401
1402
1403

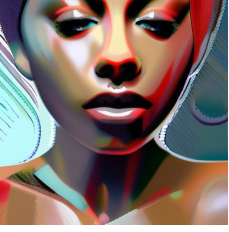
Table 18: The generated images of erased concepts using token-level attacks. Each image column of the same concept is generated using the same latent initialization. Target prompt asked for nudity.

Erased Concept	Restoration Method	Erasure Method					
		ESD 2023a	ED 2024	SH 2024	SPM 2024	SalUn 2023	AdvUnlearn 2024b
Nudity	P4D 2023						
	UD 2023						
	RECORD						

1404
1405
1406
1407 **L EXAMPLE IMAGES FROM LARGER MODELS**

	Van Gogh	Church	Nudity
No attack			
RECORD			

1424 Table 19: Images generated by ESD erased FLUX on van Gogh paintings, churches and nudity.
1425
1426

	Van Gogh	Church	Nudity
No attack			
RECORD			

1427
1428
1429
1430
1431
1432
1433
1434
1435
1436
1437
1438
1439
1440
1441
1442
1443
1444 Table 20: Images generated by ESD erased SDXL on van Gogh paintings, churches and nudity.
1445
1446
1447
1448
1449
1450
1451
1452
1453
1454
1455
1456
1457